Inorganic Chemistry

Article

pubs.acs.org/IC

Rational Design of Selective Organoruthenium Inhibitors of Protein Tyrosine Phosphatase 1B

Jun Xiang Ong,[†] Chun Wei Yap,[‡] and Wee Han Ang*[,†]

[†]Department of Chemistry, National University of Singapore, 3 Science Drive 3, Singapore 117543

[‡]Department of Pharmacy, National University of Singapore, 18 Science Drive 4, Singapore 117543

Supporting Information

ABSTRACT: Protein tyrosine phosphatases (PTPs) belong to a large family of important regulatory enzymes involved in vital mammalian signaling pathways. Selective inhibitors of PTPs are highly valuable from a therapeutic standpoint given their association with various pathological conditions. One such target is PTP-1B which has previously been linked to diabetes and cancer. However, developing a selective inhibitor against PTP-1B has proven to be daunting because the enzyme shares a high degree of structural homology with TC-PTP, an essential PTP involved in modulating immune functions. To address this challenge, a series of organoruthenium complexes was developed to bind at the PTP substrate-binding site while simultaneously target the peripheral structural space. By capitalizing on the potential difference in the structural environment proximal to the active site between different PTPs, selectivity toward PTP-1B over TC-PTP was improved, paving the way for organoruthenium complexes as selective PTP-1B metalloinhibitors.

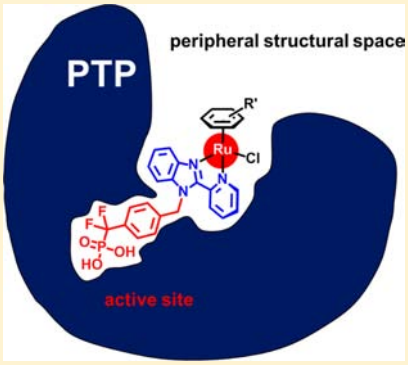

INTRODUCTION

Protein tyrosine phosphatases (PTPs) belong to a large family of 107 enzymes that play a vital role in the regulation of various signaling transduction pathways in mammalian systems.[1] PTP enzymes catalyze the dephosphorylation of phosphotyrosine (pTyr) residues, and in conjunction with protein tyrosine kinases (PTKs), they are responsible for managing the levels of phosphorylation within the cells.[2] Studies have shown that dysregulation of PTP can lead to several pathological conditions including diabetes, obesity, cancer, and autoimmune disorders.[3] Among the members of the PTP family, PTP-1B is a key negative regulator of the insulin and leptin signaling pathways associated with obesity and diabetes. PTP-1B is responsible for dephosphorylation of activated insulin receptor or insulin receptor substrates in insulin signaling,[4] as well as JAK2 which is downstream of the ObR receptor in the leptin signaling pathway.[5] Cell cultures and gene coding studies have also shown that aberrant expression of PTP-1B can contribute to obesity and diabetes.[6] Experiments on PTP-1B knockout mice showed, for instance, that PTP-1B deficiency leads to increased sensitivity toward insulin and resistance to diet-induced obesity.[7] This suggests that inhibition of PTP-1B can potentially address insulin resistance and obesity.[8]

The highly conserved enzymatic active site across the PTP family poses a major challenge in the design of selective PTP inhibitors.[1a] The signature sequence motif CX_5R can be found among the PTP active sites and is responsible for catalyzing the dephosphorylation of pTyr.[2b] In addition, PTP-1B shares 80% structural homology with TC-PTP in their catalytic domains.[9] TC-PTP is widely distributed throughout the body and is responsible for modulating immune functions.[10] As observed in TC-PTP deficient mice at 3−5 weeks of age *in vivo*, using a nonselective PTP-1B inhibitor that also acts on TC-PTP can lead to severe side effects with increased mortality.[11] Developing inhibitors with high selectivity toward PTP-1B and not TC-PTP remains a daunting task.

So far, several metal complexes have been investigated as potential PTP inhibitors. A series of Schiff-base vanadium and copper complexes was found to be very potent PTP inhibitors. However, low selectivity was observed between PTP-1B and TC-PTP.[12] These vanadium and copper Schiff-base complexes exhibited only 2-fold and 3−4-fold selectivity toward PTP-1B over TC-PTP, respectively. Recently, a library of gold−phosphine complexes was screened, and several were found to exhibit good PTP-1B inhibitory activity with varying levels of selectivity.[13] Their mechanisms were not expounded, but given the affinity of these metal centers, especially Au, toward S-containing Cys residues within the enzyme active site, it is possible that the metal centers directly reacted with Cys, thus accounting for the poor selectivity between the two enzymes. There are also several other examples of inhibitors covalently bonded to the active site by design.[14] Nevertheless, a metalloinhibitor that is designed to be selective toward PTP-1B remains elusive. Meggers showed that highly selective active-site inhibitors of PTKs can be prepared using a known kinase inhibitor, staurosporine, as a template.[15] By replacing the glycoside motif with an organoruthenium fragment, improved inhibitory profiles against specific PTKs were achieved.[16] In this manner, the octahedral Ru(II) framework provided the scaffold

Received: August 28, 2012
Published: November 2, 2012

   dx.doi.org/10.1021/ic301884j | *Inorg. Chem.* 2012, 51, 12483−12492

upon which ligands could be structurally organized.[17] This strategy yielded some of the most efficacious PTK inhibitors reported.

We were interested in combining these principles with metal−ligand interactions for rapid assembly to the design of PTP inhibitors. PTPs present a different challenge since their active sites are small and they are only capable of binding the pTyr motif. PTKs, in contrast, have a large cleft capable of accommodating a bulky ATP substrate. Since PTPs exhibit high substrate specificities even though their active sites are highly conserved, we reasoned that the space peripheral to the PTP active site must be important for their molecular recognition. Consequently, we sought to develop metalloinhibitors that are selective toward specific PTPs by capitalizing on the potential difference in the structural environment proximal to the active site. In this study, we report a class of organoruthenium PTP inhibitors with low micromolar level inhibitory constants toward PTP-1B and exhibit a 10-fold selectivity toward PTP-1B over TC-PTP.

RESULTS AND DISCUSSION

Design Approach. Due to the highly conserved nature of the PTP enzymatic active sites, targeting them directly to achieve selectivity would not be feasible. Our strategy was to target the structural space at the periphery of the active site in order to exploit differences in this environment between different PTPs. The approach was to construct metalloinhibitors that could bind to the active site while simultaneously being able to interact with the structural space proximal to the active site (Figure 1). Hence, we tethered the phenyl-

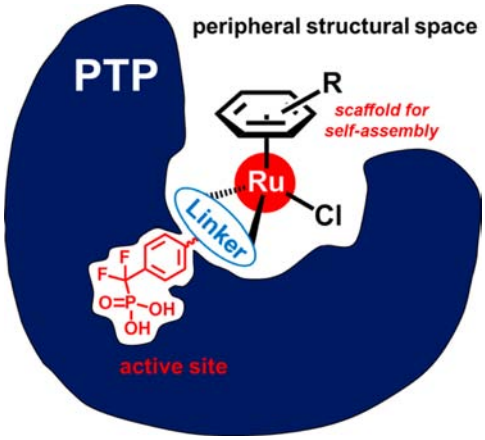

Figure 1. Approach to designing Ru(II)-based PTP inhibitors.

difluoromethylphosphonic acid (PFP) motif to bulky organoruthenium scaffolds via imidazole linkers. The PFP motif, being a nonhydrolyzable mimetic of pTyr, had been previously reported to bind PTP active sites effectively.[18] The organoruthenium fragment comprised ligands capable of interacting with the peripheral hydrophobic amino-acid residues. The Ru(II) center, in addition, served a structural role to organize these ligands in the three-dimensional space. Owing to its octahedral coordination geometry, the rigid Ru(II) scaffold offered new structural possibilities not easily achievable in purely organic molecules. Consequently, we coupled the organoruthenium fragment and the PFP group with a bidentate pyridiyl-imidazole linker for improved synthetic expediency in order to exploit the principle of chelation to rapidly bind the PFP ligand to Ru(II). In this manner, a panel of structurally diverse metalloinhibitors was easily assembled using different predefined metal precursors and PFP ligands which could then be screened for PTP selectivity.

Synthesis and Characterization. The ligands **1**−**4** were synthesized from *p*-tolualdehyde as shown in Scheme 1. *p*-Tolualdehyde was first treated with diethylphosphite in the presence of a catalytic amount of base to give the hydroxyl-phosphonate ester **P1**. Subsequent oxidation of **P1** with Dess−Martin periodinane (DMP) afforded the keto-phosphonate ester **P2**. Treatment of compound **P2** with diethylaminosulfur-trifluoride (DAST) resulted in the replacement of the ketone functional group by geminal fluorine atoms to give the difluoromethylphosphonate ester **P3**. It was reported that **P3** could be synthesized directly via Shibuya coupling using 4-iodotoulene and diethyl(bromodifluoromethyl)phosphonate with Zn dust and CuBr as coupling agents.[19] However, after repeated unsuccessful attempts, the described three-step approach was adopted. Bromination was first carried out on **P3** with *N*-bromosuccinimide (NBS) in the presence of azobisisobutyronitrile (AIBN) as the catalyst. The bromination reaction resulted in the formation of both monobrominated **P4** as the major product, as well as a dibrominated side product which could not be effectively separated. However, only **P4** reacted with the 2-(2-pyridyl)imidazole and 2-(2-pyridyl)-benzimidazole to afford the desired ligands **1** and **3**, respectively, in good yields. The dibrominated side-product remained unreacted and was removed by flash-column chromatography. Treatment of **1** and **3** with *N*,*O*-bis-(trimethylsilyl)trifluoroacetamide (BSTFA) and iodotrimethyl-silane (TMSI) followed by methanol resulted in the hydrolysis of the phosphonate ester groups to give phosphonic acids **2** and **4**, respectively, as the desired ligands.

The reaction of $[(\eta^6\text{-arene})RuCl_2]_2$, where arene = cymene or 1,3,5-triisopropyl-benzene (TIPB), with 2 equiv of imidazole-diethylphosphonate ester **1** yielded mononuclear Ru(II) complexes **1a** and **1b**, whereas treatment with imidazole-phosphonic acid **2** yielded **2a** and **2b**. The reaction was promoted by the formation of the stable 5-membered chelate between the bidentate pyridyl-imidazole ligands and the Ru(II) center. Increased steric encumbrance afforded by the larger TIPB arene did not adversely affect the formation of the complexes. After anion exchange using NH_4PF_6, **1a**,**b** were obtained as monocationic Ru(II) $[PF_6]$ complexes. Anion exchange was necessary to improve the yields and purity of the products. Complexes **2a**,**b** were isolated directly from the reaction mixture without anion exchange. Under similar reaction conditions, benzimidazole-diethylphosphonate ester **3** and benzimidazole-phosphonic acid **4** gave organoruthenium complexes **3a**,**b** and **4a**,**b** in good yields. All complexes were obtained as yellow or orange-yellow solids. Complexes with the diethylphosphonate ester groups, namely **1a**,**b** and **3a**,**b**, were soluble in moderately polar organic solvents such as dichloro-methane, chloroform, methanol, DMSO, and acetone. In contrast, **2a**,**b** and **4a**,**b** were soluble only in polar solvents such as methanol and DMSO, presumably due to the highly polar phosphonic acid groups. Notably, all of the synthesized Ru(II) complexes were soluble in aqueous conditions to concentrations exceeding 1 mM, an attribute that was important in subsequent biological investigations.

The compounds were analyzed by ^1H, $^{31}P\{^1H\}$, and $^{19}F\{^1H\}$ NMR, ESI-MS, and RP-HPLC. A distinct feature of the Ru(II)−arene complexes was the presence of resonances at 5−

dx.doi.org/10.1021/ic301884j | Inorg. Chem. 2012, 51, 12483−12492

Scheme 1

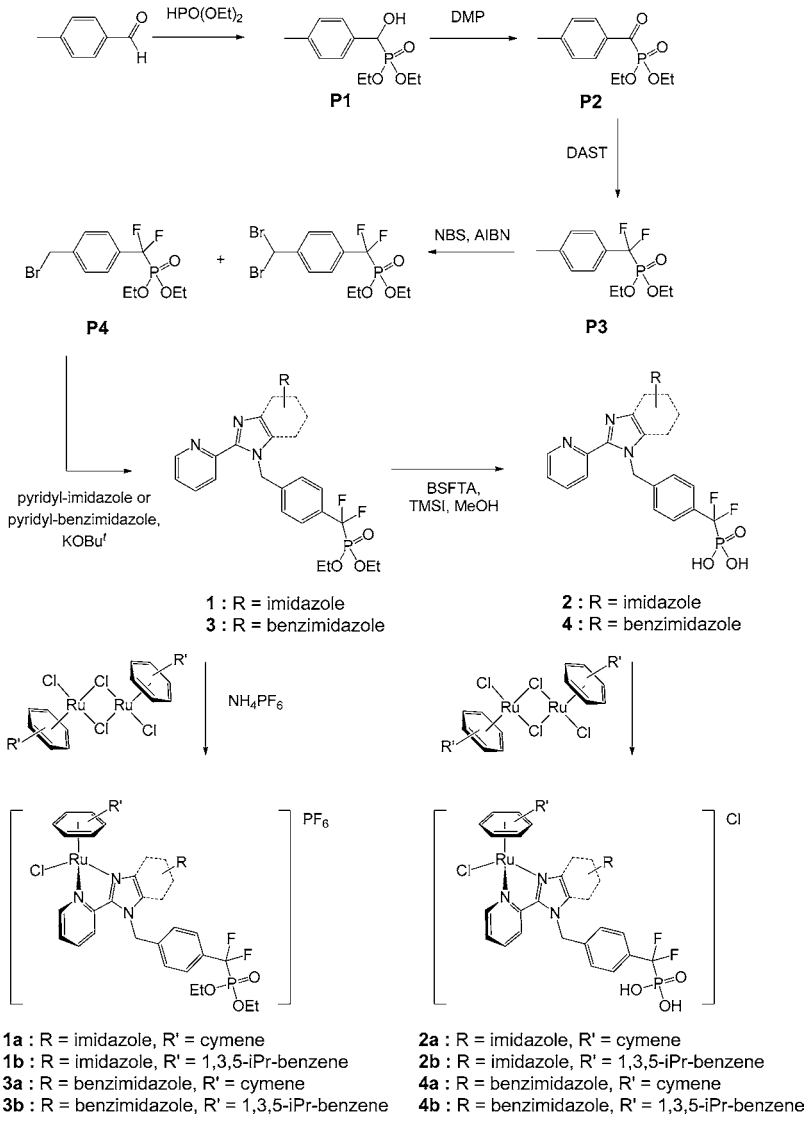

6 ppm due to the aryl-CH protons of the facially bound arene ligand. The resonances were shifted upfield from the aromatic region, indicating a more shielded environment in the presence of the metal center. In addition, the arene protons of the cymene ligand of **1a**−**4a** could be observed as 4 sets of doublets, compared to two sets of doublets of the precursor, due to the presence of diastereomers. Likewise, the six methyl protons on the isopropyl group were observed as 2 sets of doublets, as opposed to a set of doublet in the precursor. This indicated that the ligands were bound at more than 1 coordination site around the metal center. Similar observations were made on **1b**−**4b** with the TIPB arene ligand. A set of triple and a set of doublet were observed in the $^{31}P\{^{1}H\}$ and $^{19}F\{^{1}H\}$ NMR, respectively, for all the complexes due to $^{2}J_{PF}$ coupling. All the complexes were observed as M^{+} parent molecular ions in the ESI-MS and confirmed with MS/MS fragmentation analysis. However, organic CHN elemental analyses did not yield results consistent with the molecular formula of the desired compounds despite using crystalline and highly purified samples. In comparison, Ru content analyses on the samples by ICP-OES were within error limits. We hypothesized that the discrepancy was due to the presence of the CF_2 group which could yield interfering HF on combustion, thus giving rise to inaccurate results.[20] Instead, we determined the purity of the newly synthesized compounds to be >95% using RP-HPLC.

Single crystals of **1b** suitable for X-ray diffraction studies were obtained via layer diffusion of diethyl ether into its methanolic solution, while **4a** was grown by slow evaporation of a methanolic solution. To the best of our knowledge, these complexes represent the first reported organoruthenium complexes containing difluoromethylphosphonate functional groups. Figures 2 and 3, respectively, depict the structures of **1b** and **4a** with atomic numbering. Table 1 shows selected crystallographic data, and Table 2 shows selected bond lengths and angles of the complexes. The pyridyl-imidazole and pyridyl-benzimidazole rings in the complexes were observed to be largely planar. Complex **4a** crystallized as a zwitterionic structure with a deprotonated monobasic phosphonate group. The negative charge on the deprotonated phosphonate group was delocalized between O1−P1−O3 with similar O1−P1 and O3−P1 bond lengths of 1.481(3) and 1.512(3) Å. The distances were consistent with a bond order of 1−2. In

dx.doi.org/10.1021/ic301884j | Inorg. Chem. 2012, 51, 12483−12492

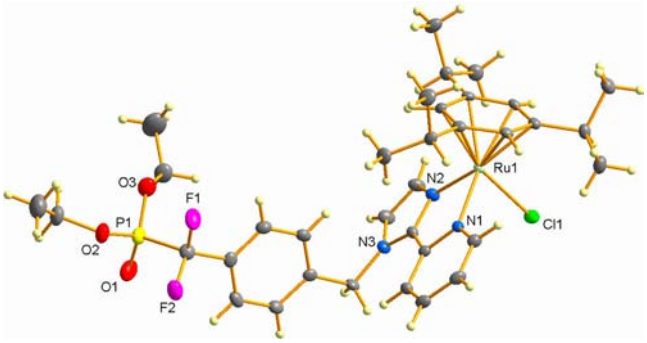

Figure 2. Molecular representation of **1b**; atoms are represented as thermal ellipsoids at 50% equiprobability. Disordered phosphonate groups and $[PF_6]^-$ anion were excluded for clarity.

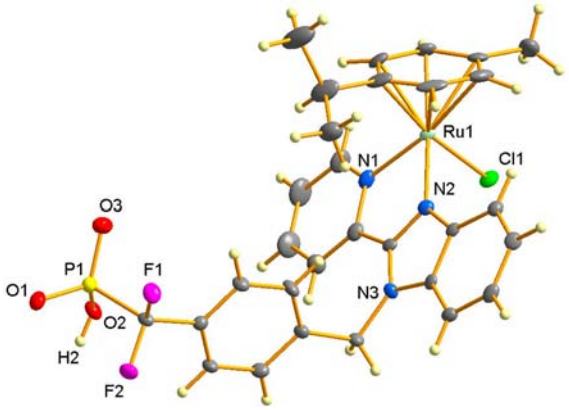

Figure 3. Molecular representation of **4a**; atoms are represented as thermal ellipsoids at 50% equiprobability. Disordered isopropyl group on the arene ligand was excluded for clarity.

comparison, the observed protonated O2−P1 bond in the crystal structure was significantly longer at 1.558(3) Å.

We investigated whether it was possible to hydrolyze the phosphonate ester groups as a facile entry to **2a**,**b** and **4a**,**b** after they have been coordinated to the Ru(II)−arene scaffold. The direct hydrolysis of phosphonate ester groups was reported for several polyaromatic Ru(II) complexes[21] but not Ru(II)−arene compounds which were more reactive and susceptible to ligand displacement. Treatment of **1a** directly with TMSI followed by methanol yielded quantitatively an unknown species with a similar ^{1}H NMR profile to **2a**. Disappearance of the ethyl peaks in the ^{1}H NMR spectrum indicated hydrolysis of the phosphonate ester group. Other resonances were largely unchanged, suggesting that organoruthenium scaffold remained intact. Closer inspection by ESI-MS analysis, however, suggested that the chloride ligand coordinated to Ru(II) was displaced by iodide, with a single peak observed at m/z 728 and corresponding to $[(\eta^6\text{-cymene})\text{RuI}(\mathbf{2})]^+$. In contrast, **2a** was previously observed by ESI-MS with a parental molecular ion at m/z 636. The source of iodide was likely decomposed TMSI reagent that was used in stoichiometric excess. Although direct hydrolysis of phosphonate groups was technically feasible, further steps would be required to convert the iodide ligand back to chloride, and the method was thus abandoned.

Aqueous Stability of Organoruthenium PTP Inhibitors. The aqueous stabilities of **3a** and **4a** were investigated using UV−vis spectroscopy over a 24 h period in water (pH 7.2) (Figure 4). There were no significant shifts in their UV−vis spectra over the period, thus indicating good aqueous stability. In the presence of 1 mM glutathione (GSH), an endogenous intracellular thiol-containing tripeptide, there was a significant blue shift in the spectra of both compounds, suggesting that organoruthenium complexes could potentially react with these nucleophiles. This shift was suppressed with the addition of 200 mM NaCl. This suggests that the aquation of the Ru−Cl bond, not degradation of the imidazole linker or phosphonate group, was important for their reactivity.[22] Under physiological conditions at high chloride concentrations, the organoruthenium complexes can be expected to maintain their good stability even in the presence of nucleophiles. Upon cell entry, where the chloride levels are lower, reaction with intracellular nucleophiles may also occur.

Inhibition of PTP-1B and TC-PTP by Organoruthenium Complexes. The organoruthenium inhibitors were designed to bind the PTP active sites using their PFP motif as a nonhydrolyzable mimetic of pTyr.[18] At the same time, the

Table 1. Selected X-ray Crystallographic Data for 1b and 4a[a]

complex	**1b**·$(C_2H_5)_2O$	**4a**·$(CH_3OH)_4$
formula	$C_{39}H_{56}ClF_8N_3O_4P_2Ru$	$C_{34}H_{45}ClF_2N_3O_7PRu$
fw	981.33	813.22
T [K]	293(2)	100(2)
wavelength [Å]	0.71073	0.71073
cryst size [mm^3]	0.36 × 0.20 × 0.10	0.36 × 0.26 × 0.10
cryst syst	triclinic	triclinic
space group	$P\bar{1}$	$P\bar{1}$
a [Å]	9.8539(4)	10.653(3)
b [Å]	13.3013(6)	12.504(3)
c [Å]	18.0943(8)	14.449(4)
α [deg]	110.4200(10)	101.457(4)
β [deg]	93.6680(10)	101.362(4)
γ [deg]	96.1320(10)	92.915(4)
V [Å^3]	2196.78(16)	1841.3(8)
Z	2	2
D_c [Mg/m^3]	1.484	1.467
μ [mm^{-1}]	0.566	0.601
θ range [deg]	1.66−27.50	1.67−27.50
no. unique data	28 789	23 737
max, min transm	0.4305 and 0.3930	0.9423 and 0.8126
R indices (all data)	R1 = 0.0524	R1 = 0.0860
	wR2 = 0.1030	wR2 = 0.1524
GOF on F^2	1.042	1.040
peak/hole [e Å^{-3}]	0.716 and −0.543	1.767 and −1.120

[a] $R = \Sigma||F_o| - |F_c||/\Sigma|F_o|$, wR2 = $\{\Sigma[w(F_o^2 - F_c^2)^2]/\Sigma[w(F_o^2)^2]\}^{1/2}$. Goodness-of-fit (GOF) = $\{\Sigma[w(F_o^2 - F_c^2)^2]/(n - p)\}^{1/2}$, where n is the number of data and p is the number of parameters refined.

Table 2. Comparison of Bond Distances [Å] and Angles [deg] of 1b and 4a

complex	**1b**	**4a**
Ru1−N1 [Å]	2.099(2)	2.103(3)
Ru1−N2 [Å]	2.080(2)	2.078(3)
Ru1−Cl1 [Å]	2.3861(7)	2.4063(12)
av Ru−C_{arene} [Å]	2.185−2.239	2.163−2.289
N2−Ru1−N1 [deg]	76.32(8)	75.68(13)
N2−Ru1−Cl1 [deg]	85.44(6)	86.12(10)
N1−Ru1−Cl1 [deg]	83.78(6)	84.66(10)
P1−O1 [Å]	1.443(2)	1.481(3)
P1−O2 [Å]	1.506(4)	1.558(3)
P1−O3 [Å]	1.635(4)	1.512(3)

dx.doi.org/10.1021/ic301884j | Inorg. Chem. 2012, 51, 12483−12492

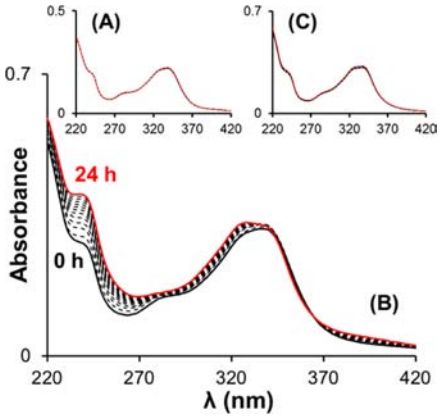

Figure 4. (A) UV−vis spectrum of **4a** in H_2O. (B) UV−vis spectrum of complex **4a** in 1 mM GSH. (C) UV−vis spectrum of **4a** in 1 mM GSH + 200 mM NaCl. The graphs are plotted in 2 h intervals over a period of 24 h.

organoruthenium scaffold would interact with amino acid residues at the periphery of the enzyme active site. By exploiting differences in this peripheral structural environment among different PTPs, selectivity toward specific PTPs can be engineered.

The compounds were subjected to an initial screen against PTP-1B and TC-PTP (Table 3) using the *p*-nitrophenylphosphate (*p*NPP). Phosphatases catalyze the hydrolysis of the phosphate group on *p*NPP to yield *p*-nitrophenol, which can be quantitated by UV−vis spectroscopy at A_{405}. The enzymes were treated with the inhibitors for 30 min before *p*NPP was added. After an incubation period of 30 min, levels of *p*-nitrophenol were determined. We took further precautions to mitigate weighing errors and the purity of metalloinhibitors by accurately determining Ru content in the stock solutions using ICP-OES and normalizing the data obtained. In addition, the same stock of organoruthenium solution was applied against two different enzymes to minimize errors arising from sample preparation. On the basis of the initial screen, compounds containing the diethylphosphonate ester ligands, namely **1**−**1b** and **3**−**3b**, were ineffective regardless of the nature of their Ru(II)−arene fragment or linker groups. Indeed, only compounds containing the phosphonic acid moiety, namely **2**−**2b** and **4**−**4b**, were efficacious. This may be attributed to increased steric encumbrance around active site-targeting moiety which prevented effective binding to the enzymatic site. In addition, it rendered the phosphonate group strongly hydrophobic and lowered their affinity toward the hydrophilic enzyme pocket.

Table 3. Initial Screening of Inhibitors against PTP-1B and TC-PTP and IC_{50} of Selected Compounds

	screening[a] [% control]		IC_{50} [μM]	
compd	PTP-1B	TC-PTP	PTP-1B	TC-PTP
1a	99.3 ± 1.7	99.7 ± 0.7		
1b	99.6 ± 0.7	100.2 ± 0.8		
2	43.4 ± 1.8	34.8 ± 1.0	72.0 ± 1.1	45.1 ± 1.0
2a	7.8 ± 0.3	45.1 ± 1.2	20.9 ± 1.0	73.4 ± 1.0
2b	7.3 ± 0.7	44.0 ± 1.6	18.7 ± 1.0	69.1 ± 1.1
3a	99.1 ± 1.9	99.4 ± 1.6		
3b	99.7 ± 0.6	100.4 ± 0.6		
4	42.8 ± 1.1	42.1 ± 2.5	68.6 ± 1.1	72.4 ± 1.0
4a	6.7 ± 0.7	57.4 ± 1.2	14.2 ± 1.0	112.1 ± 1.1
4b	7.0 ± 0.3	56.5 ± 0.6	16.6 ± 1.0	108.7 ± 1.1
5	99.5 ± 0.9	99.4 ± 1.2		
6	100.6 ± 1.3	100.1 ± 0.9		

[a]Screening was performed at inhibitor concentration of 100 μM.

Because the inhibitor contained a second-row transition metal with a known affinity toward soft nucleophiles, e.g., Cys, we investigated whether the Ru(II)−arene fragment could itself inhibit enzymatic activity directly. Therefore, [(η^6-cymene)Ru(pyridylimidazole)Cl]PF_6 (**5**) and [(η^6-cymene)Ru(pyridylbenzimidazole)Cl]PF_6 (**6**), which modeled the organoruthenium-imidazole and organoruthenium-benzimidazole fragments, respectively, and did not contain the PFP motif, were prepared and evaluated. Their inhibitory activities against both enzymes were completely abrogated, thus indicating that the organoruthenium imidazole/benzimidazole components themselves cannot inhibit PTP through allosteric interactions. In addition, it was evident from the single concentration screen (100 μM) that PFP ligands **2** and **4** were equally efficacious against both PTP-1B and TC-PTP. After incorporation of the organoruthenium scaffold, selectivity toward PTP-1B was drastically improved. A more detailed investigation was carried out by examining the dose−response of the organoruthenium inhibitors against both PTP enzymes (Figure 5) by determining the concentration at which the enzymatic activity was reduced to 50% level (IC_{50}) versus untreated controls (Table 3). On the basis of the IC_{50} values, the metalloinhibitors were 7−10-fold more effective against PTP-1B than TC-PTP, while uncoordinated PFP ligands were relatively unselective. This improved selectivity could be due to favorable interactions of the Ru(II) scaffold with amino-acid residues surrounding the active site in PTP-1B, thus leading to better binding of the complexes in PTP-1B.

Docking studies were carried out against PTP-1B (PDB ID: 2F71) using **4** and **4a** to establish the mode of binding to the target enzyme. The structure, reported by Klopfenstein, was determined at 1.55 Å resolution, and it contained a bound tetrahydroisoquinolinyl-sulfamic acid inhibitor. The inhibitor was vacated, and a simulation cell was defined around and extended for 6 Å beyond the substrate binding site. The solid state structure of **4a**, unambiguously determined using single crystal X-ray diffraction analyses, was used for the docking studies. Since the docking software was unable to process a multivalent metal center, such as Ru, the relative positions of the cymene ligand were affixed to the benzimidazole ligand by using a carbon atom to simulate the metal center. The remaining atoms in the benzimidazole-phosphonic acid fragment were unrestrained. This workaround was not expected to affect the validity of the docking results significantly since the Ru(II)−arene fragment served a structural role and since the Ru atom was also not expected to directly interact with the protein. Our model also assumed that the cymene ligand was locked to a specific orientation even though in practice it would be freely rotatable about the metal−arene centroid axis. The structure of **4** was obtained by deleting the Ru(II)−arene fragment of **4a** and was not constrained. The docking results revealed that the energetically favored conformation of **4** and **4a** involved their PFP motifs occupying the substrate-binding sites with the benzimidazole fragments directed toward the solvent region (Figure 6). These conformations were in good agreement with our design to position the bulky organoruthenium fragment at the periphery of the substrate-binding

dx.doi.org/10.1021/ic301884j | *Inorg. Chem.* 2012, 51, 12483−12492

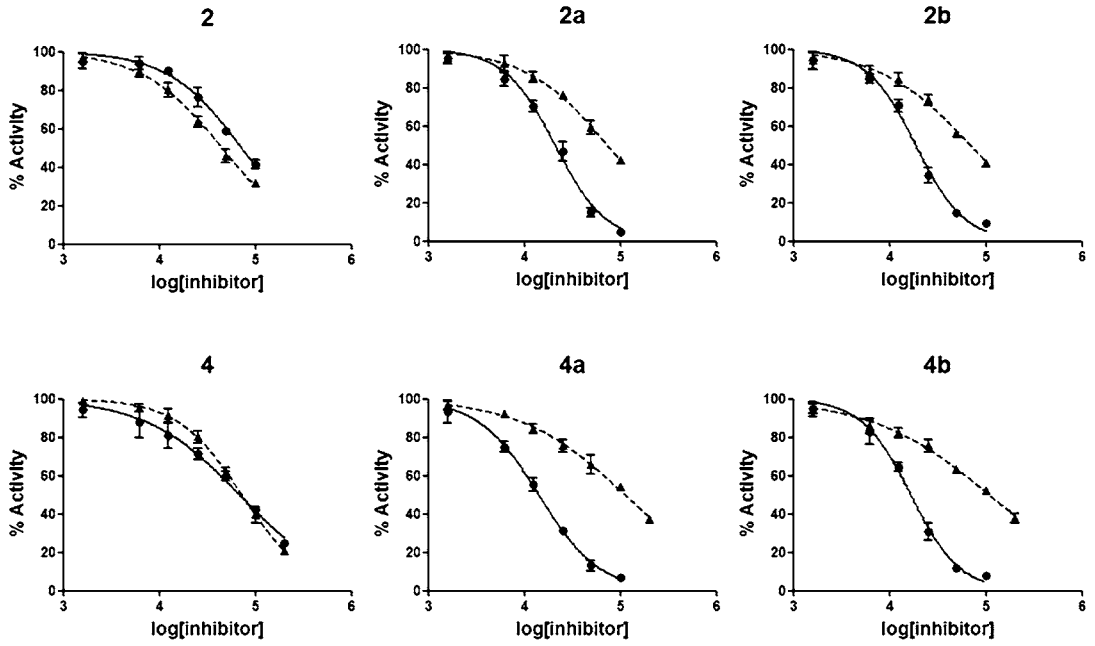

Figure 5. Dose–response curves of inhibition of compounds toward PTP-1B (bold) and TC-PTP (dotted).

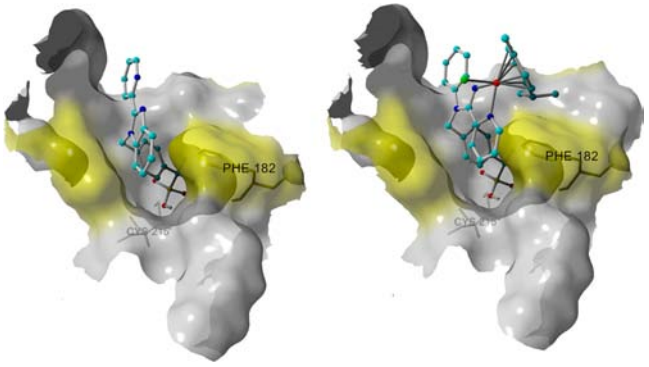

Figure 6. Conformation of parent ligand **4** in PTP-1B substrate binding site (left); conformation of **4a** in PTP-1B substrate binding site (right). The hydrophobic regions around the phosphatase substrate binding site are highlighted in yellow.

site using the PFP motif as the directing group. The methylene group between PFP and the benzimidazole linker also acted as a hinge to orientate the bulky benzimidazole group at ca. 120° from the entrance of the binding site. Because this orientation would position the isopropyl group on cymene ligand of **4a** to within 3.36 Å of Phe182, we speculated that it would give rise to favorable π-CH interaction with phenyl ring, thereby enhancing binding of **4a** to the enzyme compared to **4**. However, without further structural evidence, we cannot rule out other enzyme–substrate interactions arising from ligand-induced conformation changes that could account for the improved **4a** potency.

On the other hand, the observed diminishing potency of the inhibitors toward TC-PTP compared to their parent ligands could be due to steric effects arising from the bulky Ru(II)–arene scaffold impeding effective binding to the active site. A similar docking study on TC-PTP could not be performed since the only crystallographic data of TC-PTP (PDB ID: 1L8K) did not contain a bound inhibitor, and hence, the residues in the active site were not oriented correctly for substrate binding. Our preliminary docking study (results not shown) showed that the phosphonic acid group was not able to

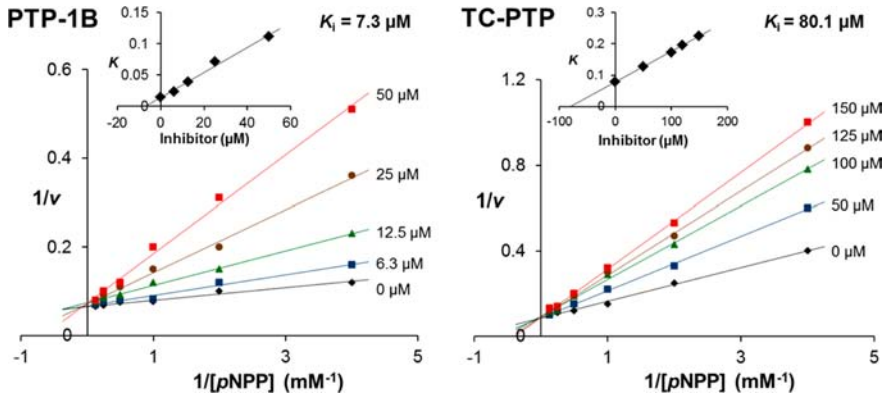

Figure 7. Lineweaver–Burk plot of $1/v$ (min μM^{-1}) vs the reciprocal of *p*NPP concentration (mM^{-1}) at five fixed concentrations of **4a** for the inhibition toward PTP-1B (left) and TC-PTP (right). K_i determination for **4a** against PTP-1B and TC-PTP (inset). The value of K_i was determined from the *x*-intercept of a plot of the slope of the line from the double-reciprocal plot as a function of inhibitor concentration (μM).

dx.doi.org/10.1021/ic301884j | *Inorg. Chem.* 2012, 51, 12483–12492

bind correctly at the active site using this structure of TC-PTP, and as a result, any data derived would not be sufficiently accurate.

From these experimental results, the presence of the Ru(II) scaffold in the structures increased potency toward PTP-1B, while the inhibition toward TC-PTP was diminished, thereby resulting in pronounced selectivities not observed in the parent ligands. Unexpectedly, the imidazole analogues were more potent in the inhibition of TC-PTP as compared to the benzimidazole counterparts. This suggests that steric effects could be used to directly tune the efficacy of the inhibitor toward TC-PTP. Detailed kinetic studies were performed to elucidate the binding modes of the complexes toward the enzymes in order to determine whether the observed differences in inhibition activities arose from different binding mechanisms toward PTP-1B and TC-PTP. Steady-state kinetic experiments with each of the enzymes were conducted with six different concentrations of *p*NPP and five different concentrations of **4a**. The Lineweaver–Burk plots (Figure 7) intersected at the same point on the $1/v$ axes, indicating a competitive mode of inhibition versus *p*NPP with inhibition constants (K_i) of 7.3 and 80.1 μM against PTP-1B and TC-PTP, respectively. Taken together, these data implied that **4a** was bound to both PTP-1B and TC-PTP at their substrate binding sites and that the different inhibition potencies were unlikely to be a result of different inhibitory mechanisms.

CONCLUSION

In summary, several Ru(II)–arene complexes were rationally designed and synthesized to be selective inhibitors of PTP-1B. Only inhibitors containing PFP groups were efficacious. Addition of the organoruthenium–arene fragments improved inhibitory activities against PTP-1B while activities against TC-PTP were diminished, leading to pronounced selectivities not observed in the parent ligands. Alone, the organoruthenium-imidazole/benzimidazole fragments were not PTP inhibitors, thus indicating that they are not solely responsible for the improved efficacies. Steady-state kinetics and molecular docking studies showed that the complexes competitively bind to the enzymes at their active sites. The results, therefore, demonstrated that molecular recognition of PTPs can be achieved by targeting both the substrate site and its periphery by applying organometallic principles of assembly and structural diversity.

EXPERIMENTAL PROCEDURES

Materials and Methods. All reagents were purchased from commercial vendors and used without further purification. Solvents were dried and distilled by standard procedures, and reactions were performed under nitrogen using standard Schlenk techniques. PTP-1B and TC-PTP were purchased from Sino-Biological. $[(\eta^6\text{-cymene})\text{-}RuCl_2]_2$,[23] $[(\eta^6\text{-TIPB})RuCl_2]_2$,[24] and 2-(2-pyridyl)imidazole[25] were synthesized according to literature methods. ^{1}H, ^{31}P, and ^{19}F NMR data were recorded on a Bruker Avance 300 or 400 MHz model. Chemical shifts are reported in parts per million relative to residual solvent peaks. Electrospray ionization mass spectra (ESI-MS) were obtained on a Thermo Finnigan MAT ESI-MS system. UV–vis spectra were recorded on a Shimadzu UV-1800 UV–vis spectrophotometer. Determination of Ru levels was carried out by CMMAC (National University of Singapore) on a Optima ICP-OES (Perkin-Elmer). Purity of Ru(II) compounds was conducted using analytical HPLC on a Shimadzu Prominence using a Shimpack VP-ODS C18 (5 μM, 120 Å, 250 mm × 4.60 mm i.d) column at r.t. at a flow rate of 1.0 mL/min with 254 nm UV detection. The gradient eluent conditions were as follows: 20–80% B over 20 min where solvent A is H_2O + 0.1% CF_3COOH and solvent B is CH_3CN + 0.1% CF_3COOH.

*Synthesis of Hydroxyl-phosphonate Ester (**P1**).* *p*-Tolualdehyde (2.34 mL, 20 mmol) was dissolved in THF (10 mL), and diethylphosphite (3.09 mL, 24 mmol) was added dropwise. Tetramethylguanidine (0.25 mL, 2 mmol) was added dropwise, and the reaction mixture was stirred at r.t. for 1 h. The reaction mixture was diluted with ethyl acetate (15 mL) and washed two times with HCl (1 M, 10 mL). The organic portion was dried over $MgSO_4$, and the solvent was removed to give the product as white solid. Yield: 4.65 g (90%). ^{1}H NMR (300 MHz, $CDCl_3$): δ 7.35 (2H, d), 7.15 (2H, d), 4.97 (1H, d), 4.05 (4H, m), 2.34 (3H, s), 1.24 (6H, t). ^{31}P NMR (121 MHz, $CDCl_3$): δ 22.3 (s).

*Synthesis of Difluoromethylphosphonate Ester (**P3**).* **P1** (516.5 mg, 2 mmol) was dissolved in dichloromethane (10 mL) and cooled to 0 °C. DMP (1.27 g, 3 mmol) was added to the solution, and the reaction mixture was stirred at r.t. for 2 h. The reaction mixture was filtered, and to the filtrate was added a solution containing $Na_2S_2O_3$ (0.5 M, 15 mL) and $NaHCO_3$ (1 M, 15 mL) and stirred for 30 min. The solution was then extracted three times with ethyl acetate (20 mL), and the organic portion was dried over $MgSO_4$. The solvent was removed to give crude **P2** as yellow oil. **P2** was redissolved in dry dichloromethane (8 mL) and cooled to 0 °C. DAST (0.53 mL, 4 mmol) was then added dropwise under nitrogen atmosphere. The reaction mixture was allowed to warm to r.t. and stirred for 12 h. Thereafter, the mixture was diluted with dichloromethane (10 mL) and ice-cold $NaHCO_3$ (1 M, 20 mL) and stirred for an additional 30 min. The reaction mixture was extracted three times with dichloromethane (15 mL), and the organic portion was dried over $MgSO_4$. The solvent was removed to give the crude compound as dark-brown oil and purified by flash column chromatography (2:3 v/v ethyl acetate:hexane, R_f = 0.7) to give the product as yellow oil. Final yield: 306.1 mg (55%). **P2** data follow. ^{1}H NMR (300 MHz, $CDCl_3$): δ 8.17 (2H, d), 7.30 (2H, d), 4.26 (4H, m), 2.39 (3H, s), 1.37 (6H, t). ^{31}P NMR (121 MHz, $CDCl_3$): δ −0.38 (s). **P3** data follow. ^{1}H NMR (300 MHz, $CDCl_3$): δ 7.50 (2H, d), 7.25 (2H, d), 4.20 (4H, m), 2.39 (3H, s), 1.31 (6H, t). ^{31}P NMR (121 MHz, $CDCl_3$): δ 7.16 (t, J_{P-F} = 118.5 Hz). ^{19}F NMR (282 MHz, $CDCl_3$): δ −31.9 (d, J_{P-F} = 118.5 Hz).

*Synthesis of Bromobenzyl Difluoromethylphosphonate Ester (**P4**).* **P3** (322.7 mg, 1.16 mmol), NBS (231.4 mg, 1.30 mmol), and AIBN (9.5 mg, 58 μmol) were dissolved in carbon tetrachloride (10 mL), and the reaction mixture was refluxed for 3 h. After the reaction, the reaction mixture was diluted with carbon tetrachloride (10 mL) and washed once with water (15 mL), $NaHCO_3$ (1 M, 15 mL), and brine (15 mL). The organic portion was dried over $MgSO_4$ to give the crude product as pale yellow oil. ^{1}H NMR analysis of the crude material indicated a mixture of starting material, monobrominated **P4**, and the dibrominated side-product in a ratio of 16:67:17%. The crude product was purified by flash column chromatography (1:2 v/v ethyl acetate:hexane, R_f = 0.8) to isolate monobrominated compound **P4** and dibrominated side-product as mixture of colorless oils. The mixture was used without further purification for the following step. **P4** data follow. Yield: 220.2 mg (53%). ^{1}H NMR (300 MHz, $CDCl_3$): δ 7.60 (2H, d), 7.48 (2H, d), 4.49 (2H, s), 4.18 (4H, m), 1.23 (6H, t). ^{31}P NMR (121 MHz, $CDCl_3$): δ 6.75 (t, J_{P-F} = 115.5 Hz). ^{19}F NMR (282 MHz, $CDCl_3$): δ −32.5 (d, J_{P-F} = 115.5 Hz).

*Synthesis of Imidazole-diethylphosphonate Ester (**1**).* The crude mixture (0.177 g containing 67% of monobrominated compound **P4**) and 2-(2-pyridyl)-imidazole (47.7 mg, 0.331 mmol) were dissolved in DMF (4 mL), and K^{t}OBu (44.6 mg, 0.40 mmol) in butanol (1 mL) was added dropwise to the reaction mixture with stirring. The reaction mixture was stirred at r.t. for 12 h. After the reaction, the solvent was removed, and the crude compound was purified by column chromatography (4:1 v/v ethyl acetate/hexane, R_f = 0.35) to give product as viscous colorless oil. Yield: 66.9 mg (48%). ^{1}H NMR (300 MHz, $CDCl_3$): 8.48 (1H, d); 8.20 (1H, d); 7.74 (1H, td); 7.53 (2H, d); 7.17–7.23 (4H, m); 7.00 (1H, d); 5.98 (2H, s); 4.15 (4H, m); 1.27 (6H, t). ^{31}P NMR (121 MHz, $CDCl_3$): δ 6.80 (t, J_{P-F} = 117.0 Hz). ^{19}F NMR (282 MHz, $CDCl_3$): δ −32.4 (d, J_{P-F} = 117.0 Hz). ESI (+ve mode) m/z 422.1 [M + H$^+$], 444.1 [M + Na$^+$].

*Synthesis of Imidazole-phosphonic Acid (**2**).* Ligand **1** (18 mg, 4.3 μmol) was dissolved in dichloromethane (3 mL), and BSTFA (57 μL, 0.214 mmol) was added to the solution. After stirring for 15 min, TMSI (30 μL, 0.214 mmol) was added to the reaction mixture. After stirring for an additional 2 h, the solvent was removed and the residue was coevaporated three times with dichloromethane (4 mL). The resulting residue was redissolved in dichloromethane (2 mL) followed by addition of methanol (10 mL) and stirred at r.t. overnight. After the reaction, solvent was removed and the residue was washed three times with water (4 mL). The residue was then suspended in water (2 mL), and NH_4OH (1 M, 1 mL) was added dropwise till the residue dissolved followed by stirring for 30 min. The solvent was removed, and the residue was washed once with dichloromethane (3 mL) and twice with diethyl ether (3 mL) to give the product as white solid. Yield: 11.0 mg (70%). ^{1}H NMR (400 MHz, D_2O): δ 8.58 (1H, d); 7.88 (1H, td); 7.67 (1H, d); 7.46 (1H, s); 7.43 (2H, d); 7.36 (1H, s); 7.18 (1H, s); 7.03 (2H, d); 5.57 (2H, s). ^{31}P NMR (162 MHz, D_2O): δ 4.98 (t, J_{P-F} = 93.0 Hz). ^{19}F NMR (376 MHz, D_2O): δ −106.2 (d, J_{P-F} = 93.0 Hz). ESI (+ve mode) *m*/*z* 366.1 ($M + H^+$); (−ve mode) *m*/*z* 364.2 ($M - H^-$).

*Synthesis of Benzimidazole-diethylphosphonate Ester (**3**).* The crude mixture (0.242 g containing 67% of monobrominated compound **P4**) and 2-(2-pyridyl)-benzimidazole (88.1 mg, 0.451 mmol) were dissolved in DMF (4 mL), and K^{t}OBu (60.7 mg, 0.542 mmol) in butanol (1 mL) was added dropwise to the reaction mixture with stirring. The reaction mixture was stirred at r.t. for 12 h. After the reaction, the solvent was removed, and the crude compound was purified by column chromatography (1:1 v/v ethyl acetate/hexane, R_f = 0.5) to give product as viscous yellow oil. Yield: 131.8 mg (62%). ^{1}H NMR (400 MHz, $CDCl_3$): 8.60 (1H, d); 8.44 (1H, dd); 7.81−7.88 (2H); 7.50 (2H, d); 7.28−7.33 (4H, m); 7.25 (2H, d); 6.23 (2H, s); 4.12 (4H, m); 1.26 (6H, t). ^{31}P NMR (162 MHz, $CDCl_3$): δ 6.21 (t, J_{P-F} = 115.8 Hz). ^{19}F NMR (376 MHz, $CDCl_3$): δ −108.3 (d, J_{P-F} = 115.8 Hz). ESI (+ve mode) *m*/*z* 472.4 [$M + H^+$], 494.4 [$M + Na^+$].

*Synthesis of Benzimidazole-phosphonic Acid (**4**).* Ligand **2** (30 mg, 63.6 μmol) was dissolved in dichloromethane (3 mL), and BSTFA (85 μL, 0.318 mmol) was added to the solution. After stirring for 15 min, TMSI (46 μL, 0.318 mmol) was added to the reaction mixture. After stirring for an additional 2 h, the solvent was removed, and the residue was coevaporated three times with dichloromethane (4 mL). The resulting residue was redissolved in dichloromethane (2 mL) followed by addition of methanol (10 mL) and stirred at r.t. overnight. After the reaction, solvent was removed, and the residue was washed three times with water (4 mL). The residue was then suspended in water (2 mL), and 1 M NH_4OH (1 mL) was added dropwise till the residue dissolved followed by stirring for 30 min. The solvent was removed, and the residue was washed once with dichloromethane (3 mL) and twice with diethyl ether (3 mL) to give the product as colorless solid. Yield: 18.2 mg (69%). ^{1}H NMR (400 MHz, D_2O): δ 8.66 (1H, d); 7.89−8.00 (2H, m); 7.78 (1H, d); 7.55 (2H, d); 7.35−7.40 (4H, m); 6.99 (2H, d); 5.85 (2H, s). ^{31}P NMR (162 MHz, D_2O): δ 5.05 (t, J_{P-F} = 92.6 Hz). ^{19}F NMR (376 MHz, D_2O): δ −106.1 (d, J_{P-F} = 92.6 Hz). ESI (+ve mode) *m*/*z* 416.2 ($M + H^+$); (−ve mode) *m*/*z* 414.3 ($M - H^-$).

*Synthesis of [(η^6-cymene)Ru(**1**)Cl]PF$_6$ (**1a**).* Ligand **1** (9.3 mg, 22.1 μmol) was dissolved in methanol (10 mL), and $[(\eta^6\text{-cymene})RuCl_2]_2$ (6.7 mg, 11 μmol) was added. The reaction mixture was stirred at r.t. for 4 h. After the reaction, solid NH_4PF_6 (3.6 mg, 22.1 μmol) was added to the reaction mixture and stirred for an additional 30 min. The solvent was removed, and the residue was redissolved in small amount of dichloromethane (2 mL) and filtered through Celite. Diethyl ether (8 mL) was added to give an orange-yellow precipitate. The precipitate was collected, washed twice with diethyl ether (6 mL), and vacuum-dried. Yield: 17.6 mg (95%). ^{1}H NMR (300 MHz, $CDCl_3$): δ 9.24 (1H, d); 7.85 (1H, t); 7.66−7.69 (2H, m), 7.59 (2H, d); 7.42 (1H, t); 7.17−7.20 (3H, m); 5.85 (1H, d); 5.78 (1H, d); 5.67 (3H, s); 5.60 (1H, d); 4.16 (4H, m); 2.79 (1H, m); 2.19 (3H, s); 1.28 (6H, t); 1.19 (3H, d); 1.17 (3H, d). ^{31}P NMR (121 MHz, $CDCl_3$): δ 6.21 (t, J_{P-F} = 114.4 Hz); −143.7 (m, PF_6^-). ^{19}F NMR (282 MHz, $CDCl_3$): δ −32.7 (d, J_{P-F} = 114.4 Hz); 3.81 (d, PF_6^-). ESI (+ve mode) *m*/*z* 692.1 (M^+, 100%). Purity (HPLC): 98.2% (based on chromatogram at 254 nm), R_t = 12.3 min.

*Synthesis of [(η^6-TIPB)Ru(**1**)Cl]PF$_6$ (**1b**).* Complex **1b** was obtained from ligand **1** (11.2 mg, 26.6 μmol) and $[(\eta^6\text{-TIPB})RuCl_2]_2$ (10.0 mg, 13.3 μmol) using the same procedure as used for **1a**. Yield: 24.0 mg (99%). ^{1}H NMR (300 MHz, $CDCl_3$): δ 9.14 (1H, d); 7.85 (1H, t); 7.68 (1H, d); 7.56−7.58 (3H, m); 7.48 (1H, t); 7.26 (1H, s), 7.16 (2H, d); 5.70 (1H, d); 5.63 (1H, d); 5.55 (3H, s); 4.17 (4H, m); 2.93 (3H, m); 1.31 (9H, d); 1.25 (9H, d). ^{31}P NMR (121 MHz, $CDCl_3$): δ 6.24 (t, J_{P-F} = 115.5 Hz); −143.7 (m, PF_6^-). ^{19}F NMR (282 MHz, $CDCl_3$): δ −32.7 (d, J_{P-F} = 115.5 Hz); 3.45 (d, PF_6^-). ESI (+ve mode) *m*/*z* 762.3 (M^+, 100%). Purity (HPLC): 99.2% (based on chromatogram at 254 nm), R_t = 15.4 min.

*Synthesis of [(η^6-cymene)Ru(**3**)Cl]PF$_6$ (**3a**).* Complex **3a** was obtained from ligand **3** (13.0 mg, 27.6 μmol) and $[(\eta^6\text{-cymene})RuCl_2]_2$ (8.4 mg, 13.7 μmol) using the same procedure as used for **1a**. Yield: 24.3 mg (99%). ^{1}H NMR (300 MHz, $CDCl_3$): δ 9.16 (1H, d); 7.86−7.94 (3H, m); 7.49−7.67 (6H, m); 7.11 (2H, d); 6.03−6.10 (3H, m); 5.87−5.93 (2H, m); 5.80 (1H, d); 4.15 (4H, m); 2.63 (1H, m); 2.61 (3H, s); 1.27 (6H, t); 1.04 (6H, d). ^{31}P NMR (121 MHz, $CDCl_3$): δ 6.23 (t, J_{P-F} = 114.4 Hz); −143.7 (m, PF_6^-). ^{19}F NMR (282 MHz, $CDCl_3$): δ −32.6 (d, J_{P-F} = 114.4 Hz); 3.84 (d, PF_6^-). ESI (+ve mode) *m*/*z* 742.1 (M^+, 100%). Purity (HPLC): 99.6% (based on chromatogram at 254 nm), R_t = 14.9 min.

*Synthesis of [(η^6-TIPB)Ru(**3**)Cl]PF$_6$ (**3b**).* Complex **3b** was obtained from ligand **3** (12.5 mg, 26.5 μmol) and $[(\eta^6\text{-TIPB})RuCl_2]_2$ (9.9 mg, 13.2 μmol) using the same procedure as used for **1a**. Yield: 24.5 mg (97%). ^{1}H NMR (300 MHz, $CDCl_3$): 9.16 (1H, d); 8.00 (1H, d); 7.89 (2H, d); 7.52−7.65 (6H, m); 7.10 (2H, d); 6.17 (1H, d); 5.87 (1H, d); 5.65 (3H, s); 4.14 (4H, m); 2.95 (3H, m); 1.26 (9H, d); 1.22 (9H, d). ^{31}P NMR (121 MHz, $CDCl_3$): δ 6.26 (t, J_{P-F} = 114.4 Hz); −143.9 (m, PF_6^-). ^{19}F NMR (282 MHz, $CDCl_3$): δ −32.6 (d, J_{P-F} = 114.4 Hz); 3.42 (d, PF_6^-). ESI (+ve mode) *m*/*z* 812.2 (M^+, 100%). Purity (HPLC): 98.6% (based on chromatogram at 254 nm), R_t = 17.8 min.

*Synthesis of [(η^6-cymene)Ru(**2**)Cl]Cl (**2a**).* $[(\eta^6\text{-Cymene})RuCl_2]_2$ (8.5 mg, 14 μmol) was dissolved in methanol (10 mL), and ligand **2** (10.2 mg, 28 μmol) dissolved in water (1 mL) was added. The reaction mixture was stirred at r.t. overnight. After the reaction, the solvent was reduced to a small volume (2 mL), and diethyl ether (8 mL) was added to give a yellow precipitate. The yellow precipitate was collected, washed once with dichloromethane (4 mL), once with ethyl acetate (4 mL), once with diethyl ether (4 mL), and vacuum-dried. Yield: 16.9 mg (90%). ^{1}H NMR (400 MHz, CD_3OD): 9.37 (1H, d), 7.94−7.98 (2H, m); 7.83 (1H, d); 7.65 (1H, s); 7.57 (2H, d); 7.50 (1H, t); 7.06 (2H, d); 6.06 (1H, d); 5.94 (1H, d); 5.77−5.81 (3H); 5.70 (1H, d); 2.59 (1H, m); 2.18 (3H, s); 1.03 (3H, d); 0.98 (3H, d). ^{31}P NMR (162 MHz, CD_3OD): δ 2.96 (t, J_{P-F} = 98.1 Hz). ^{19}F NMR (376 MHz, CD_3OD): δ −109.1 (d, J_{P-F} = 98.1 Hz). ESI (+ve mode) *m*/*z* 636.1 (M^+, 100%). Purity (HPLC): 95.6% (based on chromatogram at 254 nm), R_t = 10.2 min.

*Synthesis of [(η^6-TIPB)Ru(**2**)Cl]Cl (**2b**).* Complex **2b** was obtained from ligand **2** (10.2 mg, 28 μmol) and $[(\eta^6\text{-TIPB})RuCl_2]_2$ (10.5 mg, 14 μmol) using the same procedure as used for **2a**. Yield: 18.3 mg (88%). ^{1}H NMR (400 MHz, CD_3OD): 9.15 (1H, d), 7.72−7.76 (2H, m); 7.61 (1H, d); 7.43 (1H, s); 7.35 (2H, d); 7.28 (1H, t); 6.84 (2H, d); 6.06 (1H, d); 5.93 (1H, d); 5.81 (3H, s); 2.87 (3H, m); 1.10 (9H, d); 1.07 (9H, d). ^{31}P NMR (162 MHz, CD_3OD): δ 3.05 (t, J_{P-F} = 99.1 Hz). ^{19}F NMR (376 MHz, CD_3OD): δ −109.0 (d, J_{P-F} = 99.1 Hz). ESI (+ve mode) *m*/*z* 706.1 (M^+, 100%). Purity (HPLC): 95.5% (based on chromatogram at 254 nm), R_t = 12.7 min.

*Synthesis of [(η^6-cymene)Ru(**4**)Cl]Cl (**4a**).* Complex **4a** was obtained from ligand **4** (12.6 mg, 30.3 μmol) and $[(\eta^6\text{-cymene})RuCl_2]_2$ (9.2 mg, 15.1 μmol) using the same procedure as used for **2a**. Yield: 20.4 mg (93%). ^{1}H NMR (400 MHz, CD_3OD): 9.54 (1H, d); 8.08−8.16 (3H, m); 7.84 (1H, d), 7.62−7.70 (3H, m); 7.53 (2H, d); 7.02 (2H, d); 6.34 (1H, d); 6.08−6.15 (3H); 6.04 (1H, d); 5.95 (1H, d); 2.43 (1H, m); 2.27 (3H, s); 0.90 (3H, d); 0.88 (3H, d). ^{31}P NMR (162 MHz, CD_3OD): δ 3.08 (t, J_{P-F} = 98.1 Hz). ^{19}F NMR (376 MHz, CD_3OD): δ −109.2 (d, J_{P-F} = 98.1 Hz). ESI (+ve mode) *m*/*z* 686.1

(M^+, 100%). Purity (HPLC): 97.4% (based on chromatogram at 254 nm); R_t = 12.2 min.

*Synthesis of [(η^6-TIPB)Ru(**4**)Cl]Cl (**4b**).* Complex **4b** was obtained from ligand **4** (12.5 mg, 30 μmol) and [(η^6-TIPB)$RuCl_2$]$_2$ (11.3 mg, 15 μmol) using the same procedure as used for **2a**. Yield: 21.4 mg (90%). ^{1}H NMR (400 MHz, CD_3OD): 9.32 (1H, d); 8.09−8.20 (3H, m); 7.63−7.85 (4H, m); 7.56 (2H, d); 7.07 (2H, d); 6.16 (1H, d); 6.03 (1H, d); 5.91 (3H, s); 2.97 (3H, m); 1.20 (9H, d); 1.17 (9H, d). ^{31}P NMR (162 MHz, CD_3OD): δ 3.07 (t, J_{P-F} = 99.5 Hz). ^{19}F NMR (376 MHz, CD_3OD): δ −109.2 (d, J_{P-F} = 99.5 Hz). ESI (+ve mode) m/z 756.2 (M^+, 100%). Purity (HPLC): 98.4% (based on chromatogram at 254 nm), R_t = 15.2 min.

*Synthesis of [(η^6-cymene)Ru(pyridylimidazole)Cl]PF_6 (**5**).* 2-(2-Pyridyl)-imidazole (7.26 mg, 50 μmol) was dissolved in methanol (10 mL), and [(η^6-cymene)$RuCl_2$]$_2$ (15.3 mg, 25 μmol) was added. The reaction mixture was stirred at r.t. for 4 h. After the reaction, solid NH_4PF_6 (8.2 mg, 50 μmol) was added to the reaction mixture and stirred for an additional 30 min. After the reaction, the solvent was reduced to a small amount (2 mL) and filtered through Celite, and diethyl ether (8 mL) was added to give an orange-yellow precipitate. The precipitate was collected, washed twice with diethyl ether (6 mL), and vacuum-dried. Yield: 26.9 mg (96%). ^{1}H NMR (400 MHz, CD_3OD): δ 9.33 (1H, d); 8.08 (1H, td); 7.97 (1H, d), 7.83 (1H, d), 7.53−7.57 (2H, m); 6.03 (1H, d); 5.94 (1H, d); 5.79 (1H, d); 5.70 (1H, d); 2.62 (1H, m); 2.15 (3H, s); 1.04 (3H, d); 0.99 (3H, d). ^{31}P NMR (162 MHz, CD_3OD): δ −144.5 (m, PF_6^-). ^{19}F NMR (376 MHz, CD_3OD): δ −74.5 (d, PF_6^-).

*Syntheis of [(η^6-cymene)Ru(pyridylbenzimidazole)Cl]PF_6 (**6**).* Complex **6** was obtained from 2-(2-pyridyl)-benzimidazole (9.8 mg, 50 μmol) and [(η^6-cymene)$RuCl_2$]$_2$ (15.3 mg, 25 μmol) using the same procedure as used for **5**. Yield: 28.7 mg (94%). ^{1}H NMR (400 MHz, CD_3OD): δ 9.48 (1H, d); 8.18−8.23 (2H, m); 8.00−8.02 (1H, m); 7.67−7.71 (2H, m); 7.51−7.58 (2H, m); 6.27 (1H, d); 6.13 (1H, d); 5.98 (1H, d); 5.95 (1H, d); 2.47 (1H, m); 2.20 (3H, s); 0.92 (3H, d); 0.91 (3H, d). ^{31}P NMR (162 MHz, CD_3OD): δ −144.5 (m, PF_6^-). ^{19}F NMR (376 MHz, CD_3OD): δ −74.5 (d, PF_6^-).

*Synthesis of [(η^6-cymene)RuI(**2**)]PF_6.* Complex **1a** (8.4 mg, 10 μmol) was dissolved in dichloromethane (5 mL), and TMSI (11 μL, 75 μmol) was added and stirred at r.t. overnight. The solvent was then evaporated, and to the residue was added methanol (10 mL). The reaction mixture was stirred at r.t. for 24 h. After the reaction, the solvent was reduced to ca. 2 mL, and diethyl ether (8 mL) was added to give a yellow precipitate. The yellow precipitate was collected, washed once with dichloromethane (6 mL), once with ethyl acetate (6 mL), twice with diethyl ether (6 mL), and vacuum-dried. Yield: 7.1 mg (81%). ^{1}H NMR (300 MHz, CD_3OD): δ 9.40 (1H, d); 7.99 (1H, s); 7.96 (1H, s); 7.89 (1H, d); 7.74 (1H, s); 7.64 (2H, d); 7.51 (1H, t); 7.13 (2H, d); 6.03(1H, d); 5.94 (1H, d); 5.88 (2H, s); 5.84 (1H, d); 5.79 (1H, d); 2.87 (1H, m); 2.47 (3H, s); 1.15 (3H, d); 1.11(3H, d). ^{31}P NMR (121 MHz, CD_3OD): δ 3.63 (t, J_{P-F} = 99.0 Hz); −144.0 (m, PF_6^-). ^{19}F NMR (282 MHz, CD_3OD): δ −33.3 (d, J_{P-F} = 99.0 Hz); 1.09 (d, PF_6^-). ESI (+ve mode) m/z 728.0 (M^+, 100%).

X-ray Diffraction Studies. X-ray data were collected with a Bruker AXS SMART APEX diffractometer using Mo Kα radiation at 223(2) K with the SMART suite of programs.[26] Data were processed and corrected for Lorentz and polarization effects using SAINT software,[27] and for absorption effects using the SADABS software.[28] Structural solution and refinement were then carried out using the SHELXTL suite of programs.[29] The structure was solved by Direct methods. Non-hydrogen atoms were located using difference maps and were given anisotropic displacement parameters in the final refinement. All H atoms were put at calculated positions using the riding model.

Molecular Docking Studies. There were 116 X-ray crystallography structures of PTP-1B available in the RCSB Protein Data Bank. Structure 2F71 was selected due to its high data quality with a resolution of 1.55 Å, R value of 0.153, and R_{free} value of 0.172. The structure was prepared using YASARA[30] by using its CleanAll, OptHydAll, CorrectIso, CorrectCis functions and then minimized using AMBER03 forcefield.[31] A simulation cell was defined using the existing ligand in 2F71, extending 6.0 Å from it. The existing ligand was then removed. The macro, dock_run.mcr, available in YASARA was used to perform the docking. This macro uses the AutoDock version in YASARA to perform 25 docking runs for both parent ligand **4** and **4a**.[32] The top docked structure for parent ligand **4** and complex **4a** were used for the analysis.

PTP Inhibition Assays and Enzymatic Kinetic Studies. PTP inhibition assays and enzymatic kinetic studies were carried out in accordance with a reported procedure, using *p*NPP as the substrate.[33] The inhibition assays were performed in buffer (20 mM MOPS, 200 mM NaCl, pH 7.2, 100 μL) on a 96-well plate. Stock solutions of the inhibitors were prepared in ultrapure water and serially diluted to concentrations of 0.03−1 mM. Ru concentrations were determined using ICP-OES. Inhibitors (0.03−1 mM, 10 μL) were incubated with enzymes (150 nM) in buffer (20 mM MOPS, 200 mM NaCl, pH 7.2, 75 μL) at r.t. for 30 min. The reaction was initiated by the addition of *p*NPP (20 mM MOPS, 10 μL) and incubated for further 30 min before being terminated using the stop buffer (1 M NaOH, 5 μL). A_{405} was recorded using a microplate reader (Tecan), and IC_{50} values were obtained by fitting the concentration-dependent inhibition curves using Prism (GraphPad). The experiments were carried out in triplicates. Solutions of the compounds were freshly prepared before each inhibition assays and Ru levels determined using ICP-OES where applicable.

Kinetic analysis was performed according to the following rate equation[34]

$$v = \frac{V_{max}[S]}{K_m\left(1 + \frac{[I]}{K_i}\right) + [S]}$$

where v = initial velocity, V_{max} is the maximum initial velocity, K_m is the Michaelis constant for the substrate, [S] and [I] for concentrations of substrate and inhibitor, and K_i is the inhibition constant, derived from the slope of the Lineweaver−Burk plots.

The initial hydrolysis rates were measured at different substrate and inhibitor concentrations. The reciprocal of the reaction rate was plotted as a function of the reciprocal of the substrate concentration for each concentration of the inhibitor. The K_i values measured at the various inhibitor concentrations were plotted against concentration of the inhibitor to calculate the inhibition constants.

■ ASSOCIATED CONTENT

Ⓢ Supporting Information

Crystallographic data (CIF) for the complexes **1b** and **4a**, NMR spectra, and HPLC chromatograms of Ru(II) complexes. This material is available free of charge via the Internet at http://pubs.acs.org.

■ AUTHOR INFORMATION

Corresponding Author

*E-mail: chmawh@nus.edu.sg.

Notes

The authors declare no competing financial interest.

■ ACKNOWLEDGMENTS

The authors thank Lip Lin Koh, Geok Kheng Tan, and Yimian Hong for performing the X-ray crystallographic analysis. The funding provided by National University of Singapore and Ministry of Education (R143-000-411-133 and R143-000-512-112 to W.H.A.) and National University of Singapore NUSAGE Bridging Grant (C148-000-005-001 to Y.C.W) is gratefully acknowledged.

■ REFERENCES

(1) (a) Zhang, S.; Zhang, Z.-Y. *Drug Discovery Today* **2007**, *12*, 373−381. (b) Alonso, A.; Sasin, J.; Bottini, N.; Friedberg, I.; Friedberg, I.;

Osterman, A.; Godzik, A.; Hunter, T.; Dixon, J.; Mustelin, T. *Cell* **2004**, *117*, 699−711.
(2) (a) Salmeen, A.; Andersen, J. N.; Myers, M. P.; Tonks, N. K.; Barford, D. *Mol. Cell* **2000**, *6*, 1401−1412. (b) Tonks, N. K. *Nat. Rev. Mol. Cell. Biol.* **2006**, *7*, 833−846.
(3) (a) Andersen, J. N.; Jansen, P. G.; Echwald, S. M.; Mortensen, O. H.; Fukada, T.; Del Vecchio, R.; Tonks, N. K.; Møller, N. P. H. *FASEB J.* **2004**, *18*, 8−30. (b) Arena, S.; Benvenuti, S.; Bardelli, A. *Cell. Mol. Life Sci.* **2005**, *62*, 2092−2099.
(4) (a) Bandyopadhyay, D.; Kusari, A.; Kenner, K. A.; Liu, F.; Chernoff, J.; Gustafson, T. A.; Kusari, J. *J. Biol. Chem.* **1997**, *272*, 1639−1645. (b) Dadke, S.; Kusari, J.; Chernoff, J. *J. Biol. Chem.* **2000**, *275*, 23642−23647.
(5) (a) Zabolotny, J. M.; Bence-Hanulec, K. K.; Stricker-Krongrad, A.; Haj, F.; Wang, Y.; Minokoshi, Y.; Kim, Y.-B.; Elmquist, J. K.; Tartaglia, L. A.; Kahn, B. B.; Neel, B. G. *Dev. Cell* **2002**, *2*, 489−495. (b) Cheng, A.; Uetani, N.; Simoncic, P. D.; Chaubey, V. P.; Lee-Loy, A.; McGlade, C. J.; Kennedy, B. P.; Tremblay, M. L. *Dev. Cell* **2002**, *2*, 497−503.
(6) (a) Di Paola, R.; Frittitta, L.; Miscio, G.; Bozzali, M.; Baratta, R.; Centra, M.; Spampinato, D.; Santagati, M. G.; Ercolino, T.; Cisternino, C.; Soccio, T.; Mastroianno, S.; Tassi, V.; Almgren, P.; Pizzuti, A.; Vigneri, R.; Trischitta, V. *Am. J. Hum. Genet.* **2002**, *70*, 806−812. (b) Echwald, S. M.; Bach, H.; Vestergaard, H.; Richelsen, B.; Kristensen, K.; Drivsholm, T.; Borch-Johnsen, K.; Hansen, T.; Pedersen, O. *Diabetes* **2002**, *51*, 1−6.
(7) (a) Elchebly, M.; Payette, P.; Michaliszyn, E.; Cromlish, W.; Collins, S.; Loy, A. L.; Normandin, D.; Cheng, A.; Himms-Hagen, J.; Chan, C.-C.; Ramachandran, C.; Gresser, M. J.; Tremblay, M. L.; Kennedy, B. P. *Science* **1999**, *283*, 1544−1548. (b) Klaman, L. D.; Boss, O.; Peroni, O. D.; Kim, J. K.; Martino, J. L.; Zabolotny, J. M.; Moghal, N.; Lubkin, M.; Kim, Y.-B.; Sharpe, A. H.; Stricker-Krongrad, A.; Shulman, G. I.; Neel, B. G.; Kahn, B. B. *Mol. Cell. Biol.* **2000**, *20*, 5479−5489.
(8) (a) Blaskovich, M. A. T. *Curr. Med. Chem.* **2009**, *16*, 2095−2176. (b) Scott, L. M.; Lawrence, H. R.; Sebti, S. M.; Lawrence, N. J.; Wu, J. *Curr. Pharm. Des.* **2010**, *16*, 1843−1862. (c) Heneberg, P. *Curr. Med. Chem.* **2009**, *16*, 706−733. (d) Zhang, Z.-Y. *Curr. Opin. Chem. Biol.* **2001**, *5*, 416−423.
(9) Lee, S.; Wang, Q. *Med. Res. Rev.* **2007**, *27*, 553−573.
(10) Doody, K. M.; Bourdeau, A.; Tremblay, M. L. *Immunol. Rev.* **2009**, *228*, 325−341.
(11) (a) You-Ten, K. E.; Muise, E. S.; Itié, A.; Michaliszyn, E.; Wagner, J.; Jothy, S.; Lapp, W. S.; Tremblay, M. L. *J. Exp. Med.* **1997**, *186*, 683−693. (b) Tiganis, T.; Kemp, B. E.; Tonks, N. K. *J. Biol. Chem.* **1999**, *274*, 27768−27775.
(12) (a) Lu, L.; Yue, J.; Yuan, C.; Zhu, M.; Han, H.; Liu, Z.; Guo, M. *J. Inorg. Biochem.* **2011**, *105*, 1323−1328. (b) Wang, Q.; Lu, L.; Yuan, C.; Pei, K.; Liu, Z.; Guo, M.; Zhu, M. *Chem. Commun.* **2010**, *46*, 3547−3549.
(13) (a) Krishnamurthy, D.; Karver, M. R.; Fiorillo, E.; Orrú, V.; Stanford, S. M.; Bottini, N.; Barrios, A. M. *J. Med. Chem.* **2008**, *51*, 4790−4795. (b) Karver, M. R.; Krishnamurthy, D.; Kulkarni, R. A.; Bottini, N.; Barrios, A. M. *J. Med. Chem.* **2009**, *52*, 6912−6918.
(14) (a) Piovan, L.; Wu, L.; Zhang, Z.-Y.; Andrade, L. H. *Org. Biomol. Chem.* **2011**, *9*, 1347−1351. (b) Han, Y.; Luo, Q.; Hao, X.; Li, X.; Wang, F.; Hu, W.; Wu, K.; Lu, S.; Sadler, P. J. *Dalton Trans.* **2011**, *40*, 11519−11529.
(15) Bregman, H.; Carroll, P. J.; Meggers, E. *J. Am. Chem. Soc.* **2005**, *128*, 877−884.
(16) Atilla-Gokcumen, G. E.; Pagano, N.; Streu, C.; Maksimoska, J.; Filippakopoulos, P.; Knapp, S.; Meggers, E. *ChemBioChem* **2008**, *9*, 2933−2936.
(17) Feng, L.; Geisselbrecht, Y.; Blanck, S.; Wilbuer, A.; Atilla-Gokcumen, G. E.; Filippakopoulos, P.; Kräling, K.; Celik, M. A.; Harms, K.; Maksimoska, J.; Marmorstein, R.; Frenking, G.; Knapp, S.; Essen, L.-O.; Meggers, E. *J. Am. Chem. Soc.* **2011**, *133*, 5976−5986.
(18) Chen, L.; Wu, L.; Otaka, A.; Smyth, M. S.; Roller, P. P.; Burke, T. R.; Denhertog, J.; Zhang, Z. Y. *Biochem. Biophys. Res. Commun.* **1995**, *216*, 976−984.
(19) (a) Yokomatsu, T.; Murano, T.; Suemune, K.; Shibuya, S. *Tetrahedron* **1997**, *53*, 815−822. (b) Yokomatsu, T.; Murano, T.; Umesue, I.; Soeda, S.; Shimeno, H.; Shibuya, S. *Bioorg. Med. Chem. Lett.* **1999**, *9*, 529−532.
(20) Fadeeva, V. P.; Tikhova, V. D.; Nikulicheva, O. N. *J. Anal. Chem.* **2008**, *63*, 1094−1106.
(21) Montalti, M.; Wadhwa, S.; Kim, W. Y.; Kipp, R. A.; Schmehl, R. H. *Inorg. Chem.* **1999**, *39*, 76−84.
(22) (a) Scolaro, C.; Hartinger, C. G.; Allardyce, C. S.; Keppler, B. K.; Dyson, P. J. *J. Inorg. Biochem.* **2008**, *102*, 1743−1748. (b) Tan, Y. Q.; Dyson, P. J.; Ang, W. H. *Organometallics* **2011**, *30*, 5965−5971.
(23) Bennett, M. A.; Huang, T.-N.; Matheson, T. W.; Smith, A. K. *Inorg. Synth.* **1982**, *21*, 74−78.
(24) Hull, J. W.; Gladfelter, W. L. *Organometallics* **1984**, *3*, 605−613.
(25) Stupka, G.; Gremaud, L.; Williams, A. F. *Helv. Chim. Acta* **2005**, *88*, 487−495.
(26) *SMART ver. 5.628*; Bruker AXS Inc.: Madison, WI, 2001.
(27) *SAINT+ ver. 6.22a*; Bruker AXS Inc.: Madison, WI, 2001.
(28) Sheldrick, G. W. *SADABS ver. 2.10*; University of Gottingen: Gottingen, Germany, 2001.
(29) *SHELXTL ver. 6.14*; Bruker AXS Inc.: Madison, WI, 2000.
(30) Krieger, E.; Koraimann, G.; Vriend, G. *Protein Struct. Funct. Genet.* **2002**, *47*, 393−402.
(31) Duan, Y.; Wu, C.; Chowdhury, S.; Lee, M. C.; Xiong, G. M.; Zhang, W.; Yang, R.; Cieplak, P.; Luo, R.; Lee, T.; Caldwell, J.; Wang, J. M.; Kollman, P. *J. Comput. Chem.* **2003**, *24*, 1999−2012.
(32) Morris, G. M.; Goodsell, D. S.; Halliday, R. S.; Huey, R.; Hart, W. E.; Belew, R. K.; Olson, A. J. *J. Comput. Chem.* **1998**, *19*, 1639−1662.
(33) Montalibet, J.; Skorey, K. I.; Kennedy, B. P. *Methods* **2005**, *35*, 2−8.
(34) Ember, B.; Kamenecka, T.; LoGrasso, P. *Biochemistry* **2008**, *47*, 3076−3084.